Available on the CMS information server CMS AN 09-0xx

CMS Analysis Note

The content of this note is intended for CMS internal use and distribution only

August 26, 2009

Measurement of the CSC Spatial Resolution with Cosmic Ray Muons

Ingo Bloch[1], Vladimir Karjavin[2], Andrew Kubik[3], Petr Moisenz[2], Vladimir Palichik[2], Victor Perelygin[2], Michael Schmitt[3], and Stoyan Stoynev[3]

[1] Fermilab
[2] JINR, Dubna
[3] Northwestern University

Abstract

The spatial resolution of the CMS Cathode Strip Chambers (CSC) has been measured using cosmic ray data taken in 2008 (CRAFT) using an offline analysis package, `CSCResiduals`. The expected behavior with charge, high voltage, position within a strip, strip width and track inclination are established. The resolution *per layer* and *per chamber* are measured and found to be close to the design values, despite the fact the high voltage setting is somewhat lower than planned.

1 Introduction

The success of any CMS physics analysis involving muons depends on achieving the design performance of several sub-detector systems, including the Cathode Strip Chambers (CSC's) which are installed in the end cap regions. A large sample of cosmic ray muons was collected in the Fall of 2008, in preparation for data taking with collisions at the LHC. This cosmic ray data sample is commonly referred to as "CRAFT" *(Cosmic Run at Four Tesla)*. The CMS apparatus, trigger and reconstruction software were all working well, providing the basis for detailed studies of the performance of many sub-detector systems, including the CSC's. The commissioning of the CSC's prior to CRAFT is documented in Ref. [1].

The CSC's have been described in detail elsewhere [2]. They measure the ϕ coordinates of muon tracks well, as the bending of the muon trajectories in the magnetic fields is mainly about the $\hat{s}$ direction, where $\hat{s}$ is a unit vector in cylindrical coordinates pointing away from the beam line. The strips describe constant ϕ values, and hence are trapezoidal in shape, like the chambers themselves. A high precision is achieved on the basis of the shape of the charge distribution on three consecutive strips; this allows an adequate measurement of the muon momentum as needed for triggering purposes.

The CRAFT data were used to study and measure the spatial resolution of the CSC's as they are meant to be operated for early physics [1]. The purpose of this study is to demonstrate that all working chambers perform as designed, before colliding beams commence. Excellent earlier studies of CSC spatial resolution can be found in Ref. [4, 5].

The following sections define what we mean by "resolution," and how we measured it. We show the expected variations of the resolution as functions of charge, position within a strip, the width of the strip, and angle. We report measured values of the resolution for all types of chambers, and then conclude.

2 Analysis

The reconstruction of muon trajectories and the measurement of the muon momentum depends critically on the spatial resolution of the chambers [2]. The most important coordinate is ϕ, so these studies are concerned with the strip measurements only. An adequate measurement of R at a given z is given by the anode wires [2].

2.1 Methodology

It is important to define "resolution" and to state how it is to be measured. The *resolution* is the typical measurement error. It is determined by the design parameters of the chamber (width of the cathode strip, distance to the anode wire plane, high voltage, anode wire radius and pitch, gas mixture, electronics noise and cross talk) as well as certain characteristics of each muon track (angle, position with respect to the center of the struck strip, and amount of charge collected), and of course the physics of multi-wire proportional chambers (electron diffusion, magnetic field influence) and the reconstruction (reduction of data and knowledge of misalignments). The distribution of hit residuals with respect to the muon trajectory can

[1] The current high voltage settings are intentionally lower than what was used for the test beam, in order to avoid aging the chambers unnecessarily during commissioning periods. This has a significant impact on the spatial resolution, as described below

[2] The reconstruction software, the chamber efficiency and the success of muon reconstruction are discussed elsewhere[6–9]

ring	chambers per ring	strips per chamber	strip width (mm)	(mrad)
ME±1/1*a*	36	48	4.11 – 5.82	3.88
ME±1/1*b*	36	64	4.44 – 7.6	2.96
ME±1/2	36	80	6.6 – 10.4	2.33
ME±1/3	36	64	11.1 – 14.9	2.16
ME±2/1	18	80	6.8 – 15.6	4.65
ME±2/2	36	80	8.5 – 16.0	2.33
ME±3/1	18	80	7.8 – 15.6	4.65
ME±3/2	36	80	8.5 – 16.0	2.33
ME±4/1	18	80	8.6 – 15.6	4.65

Table 1: selected relevant physical specifications of the cathode strip chambers. The ME±1/1 chambers have a split cathode, with 64 strips at larger radii, and 48 strips at smaller. For more information, see Ref. [2, 3]

give a good measure of the resolution. A *residual* is the difference between the measured coordinate and the true or estimated true (i.e., predicted) coordinate.

For the purposes of the study, the coordinate of interest is the coordinate measured by the strips. In global coordinates, this would be $R\phi$ as measured in centimeters, but most of the studies are couched in *strip coordinates*. The strip coordinate, s, is the $R\phi$ coordinate relative to the center of the strip divided by the strip width at the position of the hit. Modulo resolution effects, one has $-0.5 \leq s \leq 0.5$. Most of the plots here will show residuals distributions in strip coordinates. In order to obtain a resolution in physical units, we multiply by the mean width of a strip in the given chamber.

The residuals distribution is not Gaussian, in general, so one must settle on a measure of the residuals distribution to be identified with the "resolution" of the given chamber. Usually we fit the distribution with a sum of two Gaussian functions, and if the resulting widths are σ_1 and σ_2, and the *areas* of the two Gaussian functions are A_1 and A_2, then we take the resolution to be:

$$\text{resolution :} \qquad \bar{\sigma} = \sqrt{\frac{A_1\sigma_1^2 + A_2\sigma_2^2}{A_1 + A_2}}. \tag{1}$$

See also Appendix B. If one Gaussian suffices, then we take simply the σ parameter of the single Gaussian. We do not take the r.m.s. as the residual distributions often have long non-Gaussian tails which inflate the r.m.s. - these tails are caused by δ-ray electrons and fall outside a discussion of the core resolution.

As defined, the resolution $\bar{\sigma}$ pertains to a hit in a *single layer*. The resolution of a chamber is more complicated, since it depends on the number of hits in the segment, the angle of the segment, the generally non-normal angle between wire groups and strips, and the fact that the strips are staggered layer-by-layer [3]. We can take the special case of segments with six hits that are normal to the chamber and pass through the center. If the residuals distribution near the edge of a strip has Gaussian width σ_e, and near the center of a strip, σ_c, then to a good approximation, the resolution for the segment is

$$\text{segment :} \qquad \sigma_{\text{seg}} = \left(\frac{3}{\sigma_e^2} + \frac{3}{\sigma_c^2}\right)^{-1/2}. \tag{2}$$

[3]There is no strip staggering in the ME1/1 chambers

We will use this expression to characterize the chamber resolution.

Another method for measuring the resolution does not rely on the residuals of a single layer, but rather on the value of χ^2 for the linear fit to all six hits. Let us define the *unweighted* χ^2 as follows:

$$\chi_0^2 \equiv \sum_{i=1}^{6} (s_i - (a + bi))^2 \tag{3}$$

where a and b are free parameters, and i plays the role of the z coordinate. Notice we have set all uncertainties to one. As a consequence, $\langle \chi_0^2 \rangle = 6\sigma_0^2$, where σ_0 is the effective uncertainty on s_i. This σ_0 parameter can be interpreted as the resolution only if non-Gaussian tails in are absent or insignificant.

It remains to explain how we make the residuals distribution. We do not have a good exterior measure of the position of the muon, so we have to use the segment itself. Perhaps the cleanest procedure is to use five out of the six hits on a good segment to predict the position of the sixth. In practice, we fit the hits in layers 1, 2, 4, 5 and 6 to a straight line to predict the "correct" position in layer 3, and then compare to the measured position in layer 3. Monte Carlo studies show that the width of the residuals distribution is inflated by about 10% due to the measurement error from the five-hit fit; this uncertainty is larger for layers 1, 2, 5 or 6. We do not remove this 10% inflation in the results reported in this note.

2.2 Expected Behavior

As stated in the Introduction, the resolution varies with four quantities:

1. the charge recorded for that hit
2. the position within the strip
3. the physical width of the strip
4. the inclination of the track

This behavior can be understood qualitatively, given a model for the formation of signals on the strips.

Analytical calculations for the formation of signals in cathode strip chambers have been available for many years. Gatti described how charge was apportioned among the strips in 1979 [10]. His calculation was updated and extended by Mathieson and Gordon in 1984 [11].

The simplest depiction of the signals on three strips as given in Fig. 1. Ignoring the time evolution of the pulses, we have simply Q_L, Q_C and Q_R, as shown. By definition, the central strip extends across $-0.5 < s < 0.5$, and the left strip is at $s = -1$ and the right, at $s = +1$. With the muon passing through the central strip at the position of the arrow, $Q_R > Q_L$, and of course $Q_C > Q_R$.

It is intuitively clear that the position of the muon relates to the relative difference $Q_R - Q_L$, and indeed the first approximation to this position is simply

$$s \approx \frac{1}{2} \frac{Q_R - Q_L}{Q_C - \min(Q_R, Q_L)}. \tag{4}$$

For a justification of this choice, see Ref. [4, 7].

The accuracy of the measurement of s depends on how well the difference $Q_R - Q_L$ can be measured. For the CSC's, most of the charge appears on the central strip, unless the muon passes quite close to the edge of the strip. For the large chambers especially, Q_R and Q_L are only a few percent of Q_C, and in the worse cases are not much larger than the pedestal width. This width characterizes the electronics noise, so the central question is: are the observed charges Q_R and Q_L larger than or comparable to this noise?

If the total charge Q is large, then the impact of the noise will be reduced. This explains why the resolution improves as Q decreases, so long as δ-ray electrons are not interfering with the charge distribution. Explicit calculations show that the resolution should be proportional to $1/Q$ [10, 11].

The charge on the right strip will increase as the muon trajectory approaches $s = 0.5$. In the limit that $s \to 0.5$, Q_L does not matter, and the approximation in Eq. 4 becomes

$$s \approx \frac{1}{2}\frac{Q_R}{Q_C} \to \frac{1}{2}$$

since $Q_R \to Q_C$ in this limit. In such a case, the electronics noise becomes relatively unimportant, since both Q_R and Q_C are substantial. In contradistinction, as the muon trajectory approaches $s = 0$, both Q_L and Q_R are minimal and therefore maximally impacted by electronics noise, making the difference $Q_R - Q_L$ relatively difficult to measure. For these reasons, one expects the best resolution for muon trajectories close to the edge of the strip, and the worst resolution when they go through the center.

The spatial distribution of the charge depends on the separation between strips, for a fixed distance between the strip plane and the anode wire plane. If the physical width of the strip is large, then Q_L and Q_R will be small. Due to the impact of electronics noise, which tends to be larger when the strips are larger, the resolution is poorer in chambers with large strips

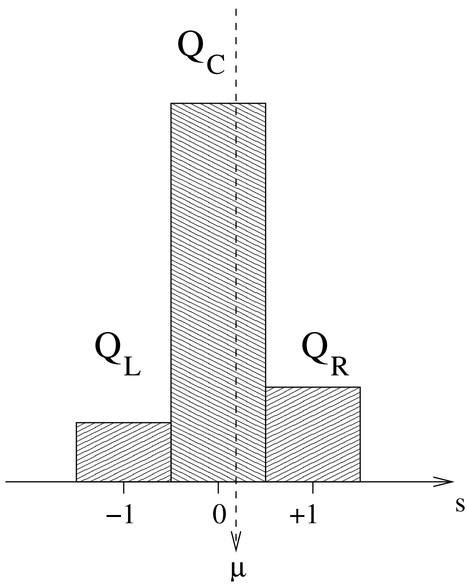

Figure 1: a notional sketch of the charge deposited on three consecutive strips. The horizontal axis is strip units, s, with the muon passing slightly to the right of zero. Three charges are registered, Q_L, Q_C and Q_R, as shown.

than in chambers with small strips. For this reason, the strips in the ME$\pm 1/1$ chambers have been made particularly small (cf. Table 1), since they play a key role in the momentum measurement in the end caps [2].

Finally, a muon which passes through the anode plane at an oblique angle (with respect to the strips) will produce a relatively broad distribution of charge across the gas gap, leading to a smearing of the distribution of charges Q_L to Q_R, and a poorer resolution.

2.3 Qualitative Results from CRAFT

The CRAFT data provide an excellent opportunity to study the point resolution of the CSC's. More than 300 M cosmic muon triggers were recorded, of which roughly 20% were generated by the CSC's. It was necessary to further filter the CSC events to obtain a sample that was useful for these studies.

An offline analysis package, `CSCResiduals`, was developed to investigate the point resolution of the CSC's. The code includes a filter to select events with good segments as well as an analysis module.

Events were selected which contained a good segment from which residuals distributions for layer 3 could be formed. A good segment was one which contained six rechits and $\chi^2 < 200$ (unreduced). An event was selected if it contained at least one good segment. In order to retain only clean events, any event with more than eight segment of any quality were rejected, as well as events with more than fifty rechits. The event was also rejected if any chamber contained more than four segments of any quality. A total of 1.58×10^3 events was selected from a subset of the CRAFT data, and about a third satisfied the further criteria specified below. The numbers of segments available for each chamber type can be found in Appendix A.

Further criteria were applied when filling residuals distributions, to ensure that the results were based on the cleanest possible segments and hits:

1. the estimated errors on the six rechits has to be smaller than 0.2 strip widths. This eliminates rechits based on a single strip or for which the cross-talk correction led to negative values for Q_R and Q_L.

2. The sum of charges for three strips and three time slices for layer three could not be too small or too large: $250 < Q_{3\times 3} < 1000$ ADC counts.

3. The segment inclination should correspond to tracks originating roughly from the interaction point:

$$-1 < \frac{dy}{dz} < -0.15 \qquad \text{and} \qquad \left|\frac{dx}{dz}\right| < 0.15 \tag{5}$$

   where these are local coordinates: dy/dz is the angle with respect to the anode wires, and dx/dz is the angle with respect to the cathode strips. (See also Ref. [8].)

4. The strip coordinates were fit to a straight line. The resulting χ^2 value were required to be less than 9 for the 5-hit fit, and less than 50 for the 6-hit fit.

These cuts were relaxed singly when checking the impact of these criteria. For further discussion of these basic criteria, see Appendix A.

In the remainder of this section, we use the CRAFT data to demonstrate the expected behavior as described in Section 2.2. No attempt was made to remove layer-by-layer misalignments, as these are known to be small compared to the resolution.

2.3.1 Resolution as a Function of Charge

The "charge" depends on several factors, including the gas composition, pressure, high voltage, amplifier gain, and of course the ionization of the gas by the muon. We denote by $Q_{3\times3}$ the sum of the charges recorded in three time bins across three consecutive strips [4, 7]. A distribution of $Q_{3\times3}$ for the CRAFT data is shown in Fig. 2. One ADC count in this figure amounts to approximately XXXXXX pC. The distribution has a long tail, similar to that expected from the Landau distribution. The overall gain, including electronics gain, varies considerably from chamber to chamber, however, so the distribution in Fig. 2 is more accurately described as a sum of many Landau distributions, with widely varying peak positions.

Residuals distributions were made for several bins in $Q_{3\times3}$ and fit individually to Gaussians. A direct comparison of the residuals distributions is shown in Fig. 3, which shows plainly that small charges give poorer resolution. One can also see that the very largest charges do not give the very best resolution, due to distortions of the charge distribution caused by δ-ray electrons.

A summary of the variation of resolution as a function of charge is given in Fig. 4. Chambers in rings ME$\pm$2/2 and ME$\pm$3/2 were selected for this plot, since they have the largest number of events in CRAFT. The cuts on the χ^2 of the 2-dimensional strip fit were relaxed for this study, so that the impact of δ-ray electrons is clear. If the cuts are imposed, then the rise for $Q_{3\times3} > 800$ ADC counts is eliminated.

In order to interpret the behavior seen in Fig. 4, we performed an *ad hoc* parametrization of the observed variation of the resolution with charge, assuming that at low charge, the variation goes as $1/Q$, that there is a constant term representing electronics noise and similar effects, and that the poorer resolution caused by δ-ray electrons rises linearly with charge. Our *ad hoc* function [4] is:

$$\sigma(Q) = \sqrt{\left(\frac{a}{Q}\right)^2 + (b + cQ)^2} \tag{6}$$

where the parameters a, b and c are to be determined by a fit. For the results shown in Fig. 4, we obtain an excellent description with $a = 11.6 \pm 0.2/(\text{ADC count})$, $b = 0.018 \pm 0.001$ and $c = (1.4 \pm 0.1) \times 10^{-5}$.

Another demonstration of the sensitivity of the resolution to charge is provided by two runs taken outside of the CRAFT exercise, in which the high voltage was raised by 50 V. Since the number of events was modest, the event and segment selection was somewhat looser than described above. Fig. 5 shows the increase in the charge and the consequent improvement in the resolution. The improvement is consistent with the expected $1/Q$ behavior.

2.3.2 Resolution as a Function of the Position Within a Strip

The resolution obtained from the measurement of Q_L, Q_C and Q_R is much better than if one simply put the hit at $s = 0$ and set the uncertainty to the strip width divided by $\sqrt{12}$. Nonetheless, the strip width does play a central role, as discussed briefly in Section 2.2. If

[4] The error calculations in the reconstruction code take into account variations of the resolution with charge, as well as with strip width and the position within a strip. The function displayed in Eq. 6 is not used.

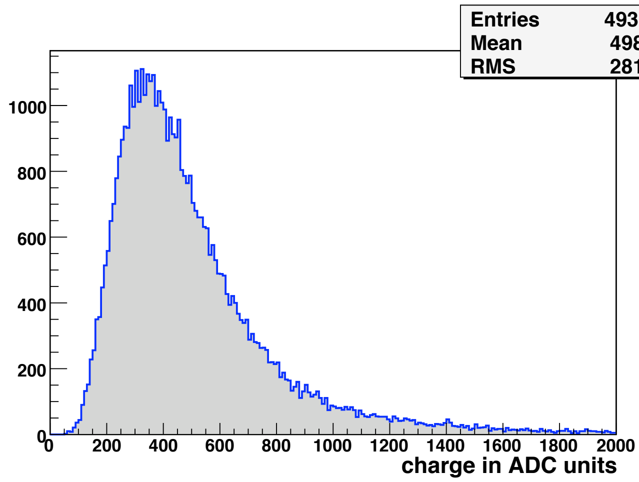

Figure 2: observed charge distribution, $Q_{3\times3}$, in ADC counts.

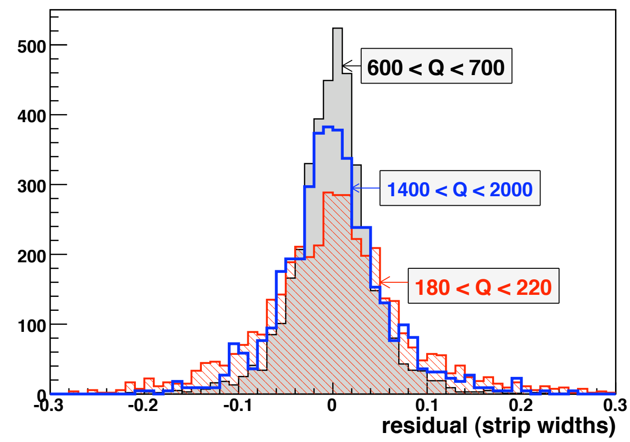

Figure 3: example residuals distributions, for three narrow ranges of charge. All three distributions are normalized to the same area

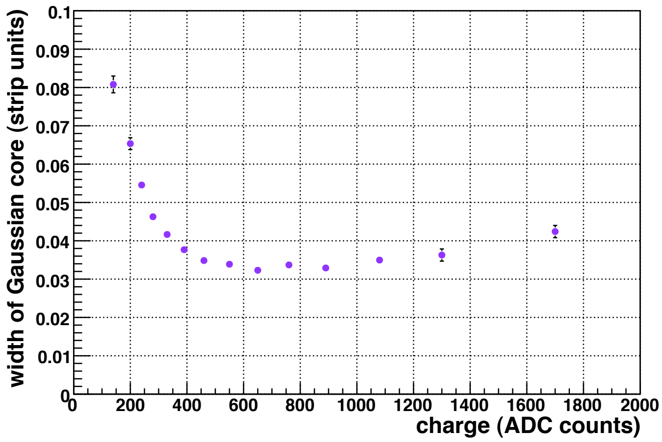

Figure 4: variation of the *per layer* resolution as a function of $Q_{3\times3}$. This measurement was made using chambers in ME$\pm$2/2 and ME$\pm$3/2; other chambers give very similar results.

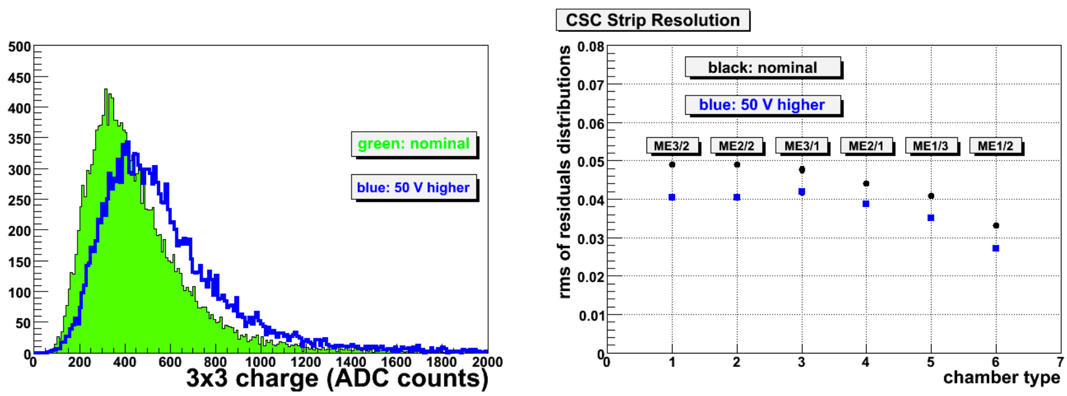

Figure 5: *Left:* charge distributions for two consecutive runs. The solid histogram corresponds to the nominal setting, and the open histogram corresponds to an increase of 50 V. *Right:* comparison of the resolution for the same two runs.

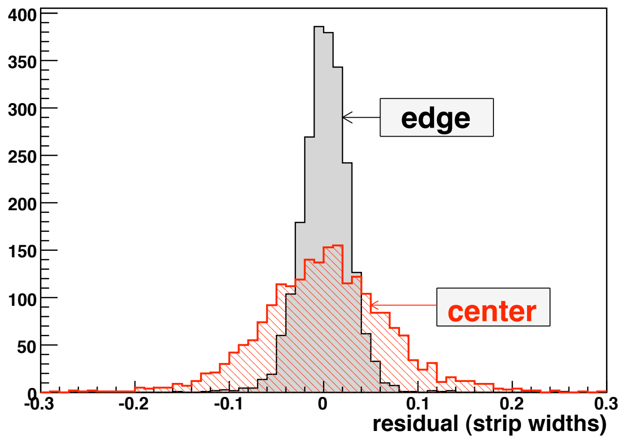

Figure 6: example residuals distributions, for muons passing near the center and near the edge of the strip

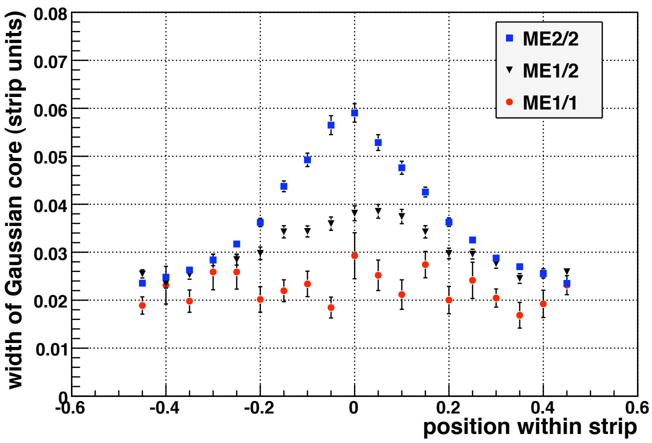

Figure 7: variation of the *per layer* resolution as a function of s, the position within the strip, for three different types of chambers

the charge is nearly the same on two consecutive strips, then the measurement is optimal; it is worse when the minimum charge is measured on the side strips. A direct comparison of the residuals distribution for two extreme cases is shown in Fig. 6. The distribution for $|s| < 0.025$ ("center") is much broader than the one for $|s| > 0.425$ ("edge").

A summary of the variation of the resolution with s is shown in Fig. 7. For the ME$\pm$2/2 chambers, the resolution in the center of the strip is worse by about a factor of two than at the edge. This variation is weaker for chambers with thinner strips, such as ME$\pm$1/2 and ME$\pm$1/1.

2.3.3 Resolution as a Function of the Strip Width

Most of the analysis is done in terms of the normalized strip width, s. The physical width of the strip matters, too. For broad strips, most of the charge is collected on the central strip,

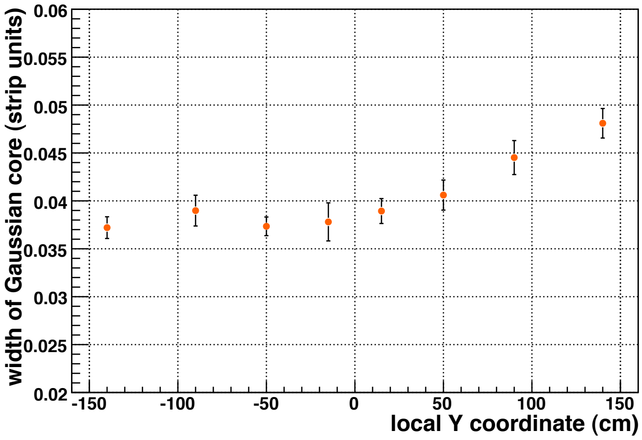

Figure 8: variation of the *per layer* resolution as a function of y, the local coordinate roughly parallel to the strips. These measurements were done with the ME$\pm 2/2$ and ME$\pm 3/2$ chambers.

leaving a small amount for Q_L and Q_R, leading to a poorer resolution. For this reason, the smaller chambers have a much better resolution than the larger chambers. Within a chamber, there is a variation of the resolution along the strip, since the strip is narrower at the narrow end of the chamber ($y < 0$) and wider at the broad end ($y > 0$). Fig. 8 illustrates this behavior for chambers from ME$\pm 2/2$.

2.3.4 Resolution as a Function of the Track Angle

The results in the previous subsections were derived for muon trajectories that were nearly perpendicular to the strips. For low-momentum muons coming from the interaction point, however, more oblique trajectories are possible. We have observed a clear variation of the resolution as a function of dx/dz in chambers from ring ME$\pm 2/2$, see Fig. 9. For all other results reported in this note, a tight cut on $|dx/dz|$ has been applied.

2.3.5 Normalized Residuals

The rechit code computes the estimated uncertainty taking variations as a function of charge, position within a strip, and strip width into account [7]. Distributions of normalized residuals (“pull distributions”) allow us to check those calculations.

Fig. 10 shows the pull distribution for all chambers. The shape is fairly Gaussian, and the fitted width is $\sigma = 1.349 \pm 0.005$, which is fairly close to the target value of 1.15. A summary of the pulls for all chamber types is given in Table 2. Overall, the pulls are too wide, especially for the ME$\pm 1/1$ chambers. It will be possible to adjust the error estimates on the basis of the CRAFT data.

2.3.6 Badly Reconstructed Segments

Most of the analysis presented in this note is directed toward the characterization of good segments reconstructed from good rechits. Some rechits are quite poor, however, and some segments have a very large χ^2. In this subsection, we present some investigations of these cases.

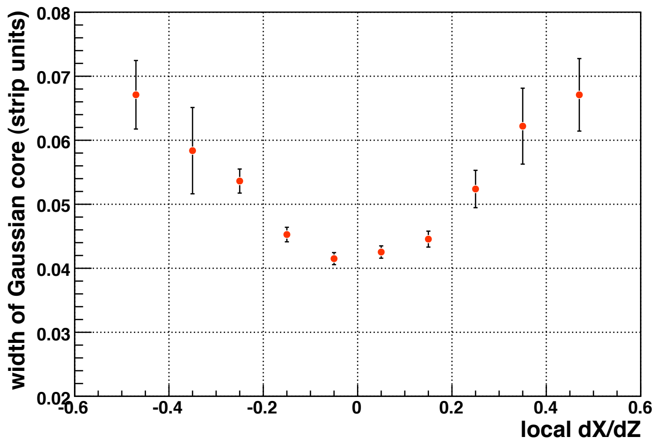

Figure 9: variation of the *per layer* resolution as a function of local dx/dz, which quantifies the segment inclination with respect to the strips. These measurements were done with the ME$\pm$2/2 chambers.

ring	width of pull distribution
ME$\pm 1/1b$	1.89 ± 0.06
ME$\pm 1/2$	1.34 ± 0.01
ME$\pm 1/3$	1.52 ± 0.01
ME$\pm 2/1$	1.28 ± 0.02
ME$\pm 2/2$	1.42 ± 0.01
ME$\pm 3/1$	1.26 ± 0.04
ME$\pm 3/2$	1.37 ± 0.02
ME$\pm 4/1$	1.17 ± 0.03

Table 2: widths of the normalized residual distributions, obtained by fitting the central core of the distribution, as in Fig. 10.

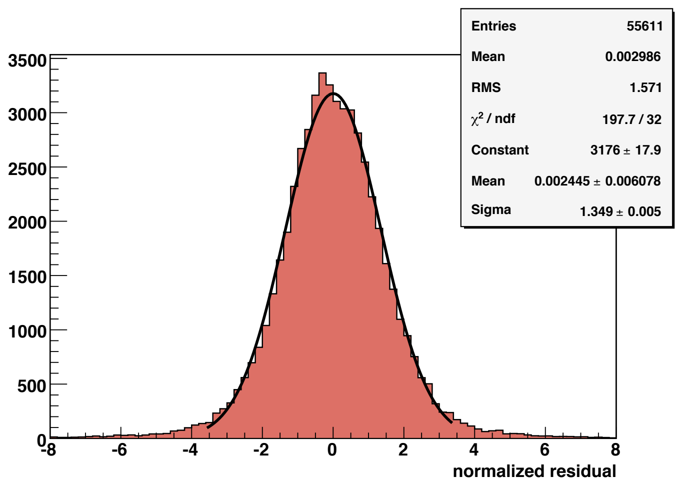

Figure 10: distribution of normalized residuals ("pull distribution") for all chambers. Also shown is a fit to a single Gaussian.

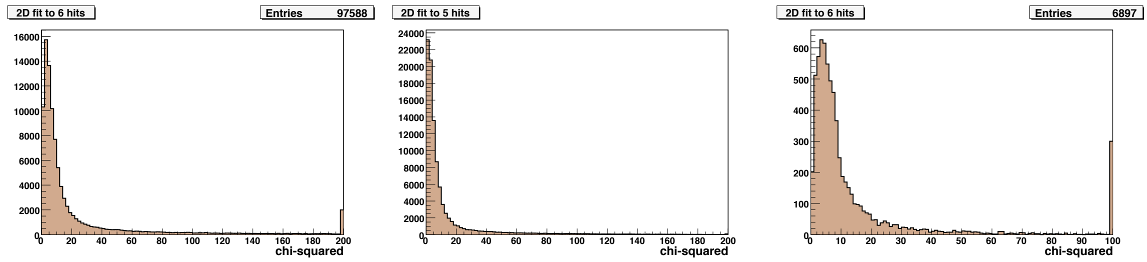

Figure 11: distributions of χ^2 values obtained by fitting the strip coordinates to straight lines. *Top:* $\chi^2_{(6p)}$ after all selection but before cuts on χ^2. *Middle:* $\chi^2_{(5p)}$. A tight cut is placed at $\chi^2_{(5p)} < 9$. *Bottom:* $\chi^2_{(6p)}$ after the tight cut on $\chi^2_{(5)}$. A loose cut is applied: $\chi^2_{(6p)} < 50$.

The bottom plot in Fig. 11 shows $\chi^2_{(6p)}$ after a tight cut on $\chi^2_{(5p)}$. The long tail is caused by bad rechits in layer 3. We applied a cut $\chi^2_{(6p)} > 100$ to select a sample of about 300 such rechits. Fig. 12 shows some interesting distributions for these bad rechits.

The first plot shows the pull distribution. Given the way these bad rechits were selected, one expects large values with an absence of small values. The next plot shows the actual residuals, which also have a hole and somewhat, but not very large values. The third plot shows that the estimated errors are quite tiny – compare with Fig. 15 which shows much larger values for more normal rechits. Thus the large pulls are caused mainly by small estimated errors. The fourth plot gives a clue why the errors might be small: the measured charge is very large – compare to Fig. 2. The very large charge may indicate a δ-ray electron or some other agent distorting the pulses on the strips. Another clue comes from the last plot, showing that the "bad" rechits are found more often near the edge of the strip, where the error should be smaller. The reconstruction code computes the estimated errors based on average behavior of the resolution as a function of charge, position within the strip and strip width. Apparently, for these peculiar rechits, there is a conspiracy of effects, namely very large charge, and a position close to the edge of a strip.

In short, for rechits near the edge of a strip, when the charge is very high, the measured coordinate might be less accurate, and the estimated error too small, leading to a very large normalized residual and a bad value for χ^2.

2.4 Measurements of the Nominal Resolution

The results in the previous section demonstrate the expected qualitative behavior of the resolution. In this section, we quantify the resolution of the CSC's, as measured with CRAFT data, in order to verify that they are performing as designed.

The cut $\chi^2 < 200$, listed in Section 2.3, is a loose cut, which could allow segments in which the fit to rechits in layers 1, 2, 4, 5 & 6 might give a poor prediction for the position in layer 3. This is why we impose a tight cut on $\chi^2_{(5p)}$ for the 5-hit, 2-dimension fit to all strips except the one from which we will obtain the residuals distribution. We studied the impact of the cut on $\chi^2_{(5p)}$ by selecting segments in ME$\pm$2/2 for which $|s| > 0.4$ in layer 3, and checking the width of the residuals distribution as the cut on $\chi^2_{(5p)}$ was tightened. See Appendix A for more information. A very loose cut is placed on $\chi^2_{(6p)}$ to remove rechits which are far off the correct position.

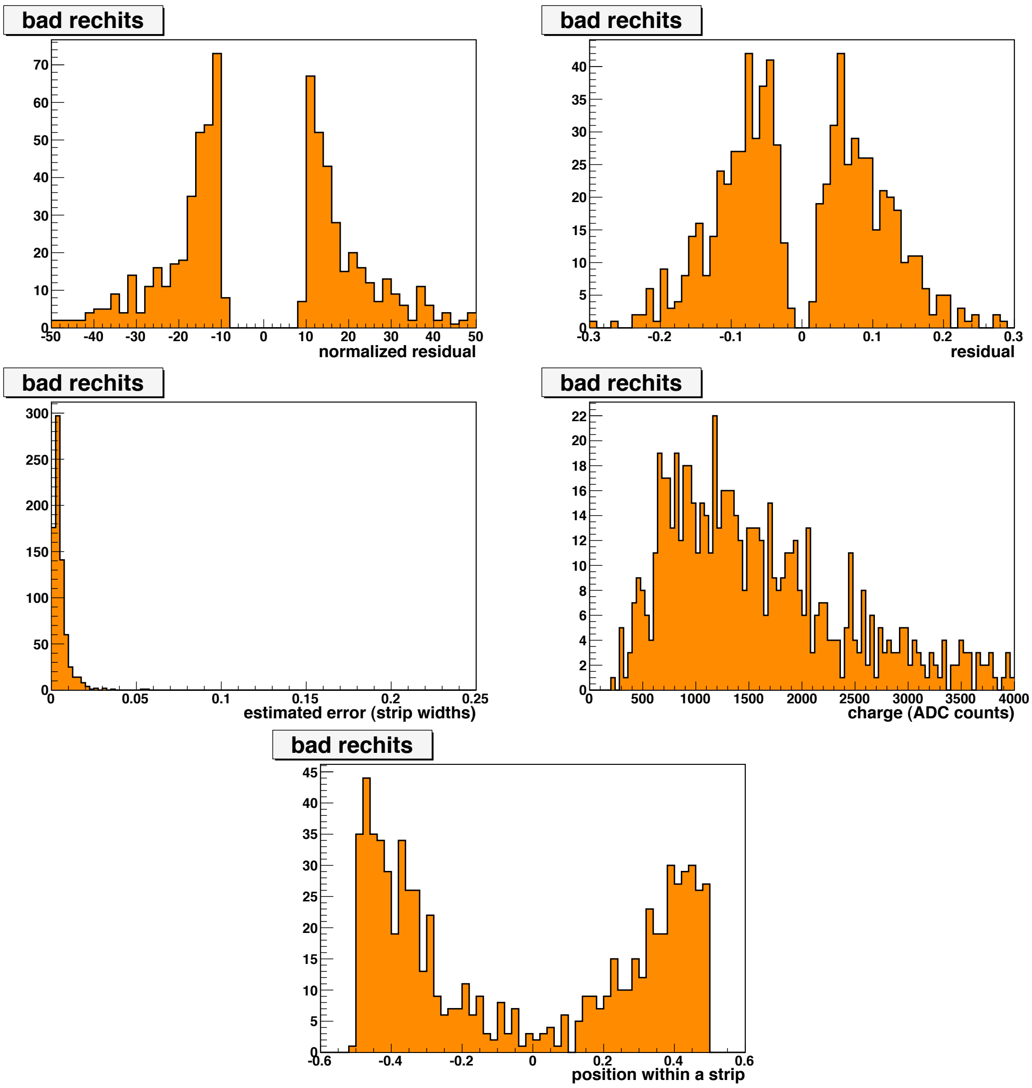

Figure 12: distributions for rechits giving $\chi^2_{(6p)} > 100$.

ring	resolution			
	fit to two Gaussians		*derived from* χ_0^2	
	strip widths	μm	strip widths	μm
ME±1/1*b*	0.024 ± 0.002	144	0.017	102
ME±1/2	0.034 ± 0.001	285	0.029	245
ME±1/3	0.044 ± 0.001	578	0.041	537
ME±2/1	0.046 ± 0.001	510	0.044	489
ME±2/2	0.040 ± 0.001	487	0.039	474
ME±3/1	0.054 ± 0.002	633	0.052	613
ME±3/2	0.044 ± 0.001	534	0.041	501
ME±4/1	0.054 ± 0.004	648	0.052	625

Table 3: resolution *per layer* for each chamber type.

ring	resolution (μm)		
	design	*per layer* / $\sqrt{6}$	Eq. 2
ME±1/1	75	59	53
ME±1/2	75	116	110
ME±1/3	150	234	194
ME±2/1	150	208	172
ME±2/2	150	199	169
ME±3/1	150	258	200
ME±3/2	150	218	182
ME±4/1	150	264	221

Table 4: resolution *per chamber* for each chamber type

Residuals distributions for chambers in each ring were fit to the sum of two Gaussians, and the resolution computed according to Eq. 1. These distributions and the fits are given in Appendix B. Table 3 lists the *per layer* resolution obtained in this manner. The values given in μm are obtained by multiplying the resolution in strip widths by the average width of the strip (see Table 1).

We formed distributions of χ_0^2 (Eq. 3) for each chamber type – some examples are given in Fig. 13. We computed σ_0 (which would be in units of the strip width) and converted to an uncertainty in μm using the average physical strip width. The results are listed in Table 3. These values are somewhat smaller than the values obtained from the fit to two Gaussians.

The resolution of a chamber, given six good rechits, can be estimated on the basis of the *per layer* resolution. One can simply take the numbers listed in Table 3 and divide by $\sqrt{6}$, or one can perform a slightly more refined analysis indicated by Eq. 2. The latter gives systematically lower values for the resolution than the former. Table 4 lists both sets of values, which can be compared to the design values [2]. In general, the observed values are somewhat higher, due in part to the 10% inflation inherent in the method, and from the fact that the high voltage setting is slightly lower than nominal.

Very similar studies have been conducted by the DUBNA group and are available already in Ref. [12]. Their selection of segments is somewhat tighter than what has been described here. For example, they applied much tighter cuts to the χ^2/NDF for the segment fit, and also for the 6-hit 2-dimension strip fit, here denoted $\chi^2_{(6p)}$. From CRAFT data they obtained a

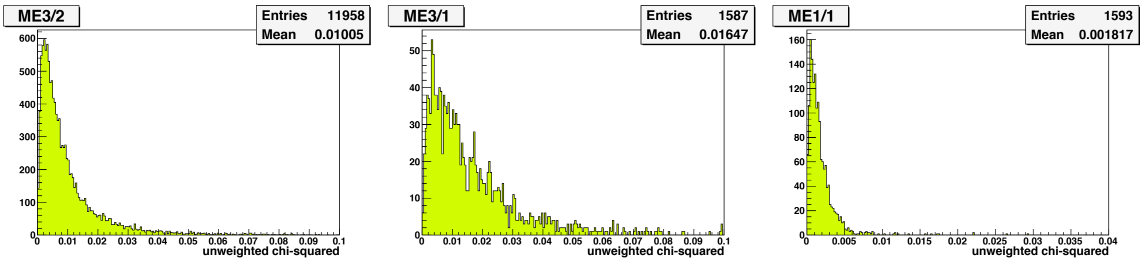

Figure 13: example distributions of χ_0^2

per layer resolution of 107 μm for ME1/1, and a *per chamber* resolution of better than 50 μm. These values are not incompatible with those listed in Tables 3 and 4. For the details of their study, see Ref. [12].

3 Conclusions

The CRAFT data have been used to study the resolution of the CSC's as a function of charge, position within a strip, strip width, and track angle, as well as to quantify the resolution of all chamber types. The expected qualitative behavior has been demonstrated. The measured resolutions of all chamber types compare reasonably well with the design values, as tabulated in Table 4, given the fact that the high voltage is set lower than originally intended.

More refined studies can be carried out in the future, either with cosmic ray muons, or, hopefully, with muons produced in pp collisions.

Acknowledgments

The approach and direction of these studies take inspiration from the earlier work by Stan Durkin (OSU) [5]. The fine work by the Florida Group also set an excellent example [4].

Appendix A

Justifications for the criteria listed in Section 2.3 are given below, based on distributions made from the output of a loose CSC skim (program `CSCSkim`, skim type 1). This skim demanded at least three chambers with hits, and at least two segments of any quality.

Fig. 14 shows the distribution of the total number of rechits in an event. Spikes corresponding to one, two and three chambers are visible. Four chambers correspond to 24 hits, except when one of them is ME$\pm$1/1a, in which case the number is 48. The cut is placed at 50. Events with very many segments come from showers, which clearly are inappropriate for these studies. A rather loose cut at 8 has been placed. Similarly, no chamber may have more than four segments. This excludes the possibility that a single chamber has a number of rechits close to 60, leading to very many three-hit segments that do not correspond to a muon track.

Given that most "messy" events are eliminated by these three cuts, we can look at the quality of the remaining segments. Fig. 14 shows the number of hits on a segment; we require six. After that cut is applied, the unreduced χ^2 distribution shows a reasonable peak around 8, with a very long tail. The plot puts all overflow entries in the bin just before 200 – these are the segments that are eliminated. These segments would also be reduced by the cut on the estimated hit errors, discussed below. Given these two cuts defining a "good" segment, the number of good segments per event is also shown. Most events contain more than one good segment, indicating that these events correspond to valid muon trajectories that are reconstructed well.

If a segment has a hit with a large uncertainty, then the segment may be unreliable, so such segments are rejected. Fig. 15 shows the distribution of the largest uncertainty of all the hits on a segment. A clear spike at $1/\sqrt{12} = 0.289$ is visible. Our criteria demand that this uncertainty be less than 0.2. For reference, Fig. 15 also shows the distribution of uncertainties for the hits in layer 3.

The prediction of the coordinate in layer 3 is likely to be poor if the 5-hit fit to layers 1, 2, 4, 5 & 6 has a bad $\chi^2_{(5p)}$. Successively tighter cuts on $\chi^2_{(5p)}$ were tried, and a stable resolution obtained for $\chi^2_{(5p)} < 10$. After this cut is applied, the incidence of extremely bad residuals is reduced by applying a loose cut on the 6-hit $\chi^2_{(6p)}$, namely $\chi^2_{(6p)} < 50$. Distributions of $\chi^2_{(5p)}$ and $\chi^2_{(6p)}$ are shown in Fig. 11.

Appendix B

The residuals distributions for all chamber types are given in this appendix. The distributions have been fit to sums of two Gaussians, with means set to zero. The function form is:

$$f(x) \equiv \frac{A_1}{\sqrt{2\pi}\sigma_1} \exp\left(\frac{-x^2}{2\sigma_1^2}\right) + \frac{A_2}{\sqrt{2\pi}\sigma_2} \exp\left(\frac{-x^2}{2\sigma_2^2}\right) \tag{7}$$

where optimal values for the parameters σ_1, σ_2, A_1 and A_2 are obtained from the fit. The resolution is defined by Eq. 1. The residuals distributions with fits are given in Fig. 16.

Another test of the position measurement is provided by the distribution of the strip coordinates themselves. Ideally, this distribution should be a flat-top box for $-0.5 < s < 0.5$. Resolution on s will round off of sides of the box. Also, some rechits coordinates cannot be calculated correctly, if one does not have three strips (sometimes there are two few or even too many) or if the cross-talk correction leads to negative values for Q_L and/or Q_R. Fig. 17 shows the distributions of s for all chamber types.

For reference, a summary of the mean charge $\langle Q_{3\times3}\rangle$ and r.m.s. pedestal width is given in Table 5. These numbers come from run quality monitoring plots produced using `CSCValidation` [13].

References

[1] R. Breedon et al., *Post-Production Testing and Commissioning of the CMS End-cap Cathode Strip Chambers*, CMS-NOTE, in preparation

[2] CMS Collaboration, *CMS – The Muon Project*, CERN/LHCC 97-32

[3] Yu V. Erchov et al., *"ME1/1 Cathode Strip Chambers,"* CMS Note 2008/026.

[4] V. Barashko et al., *Fast Algorithm for Track Segment and Hit Reconstruction in the CMS Cathode Strip Chambers*, CMS NOTE-2007/023

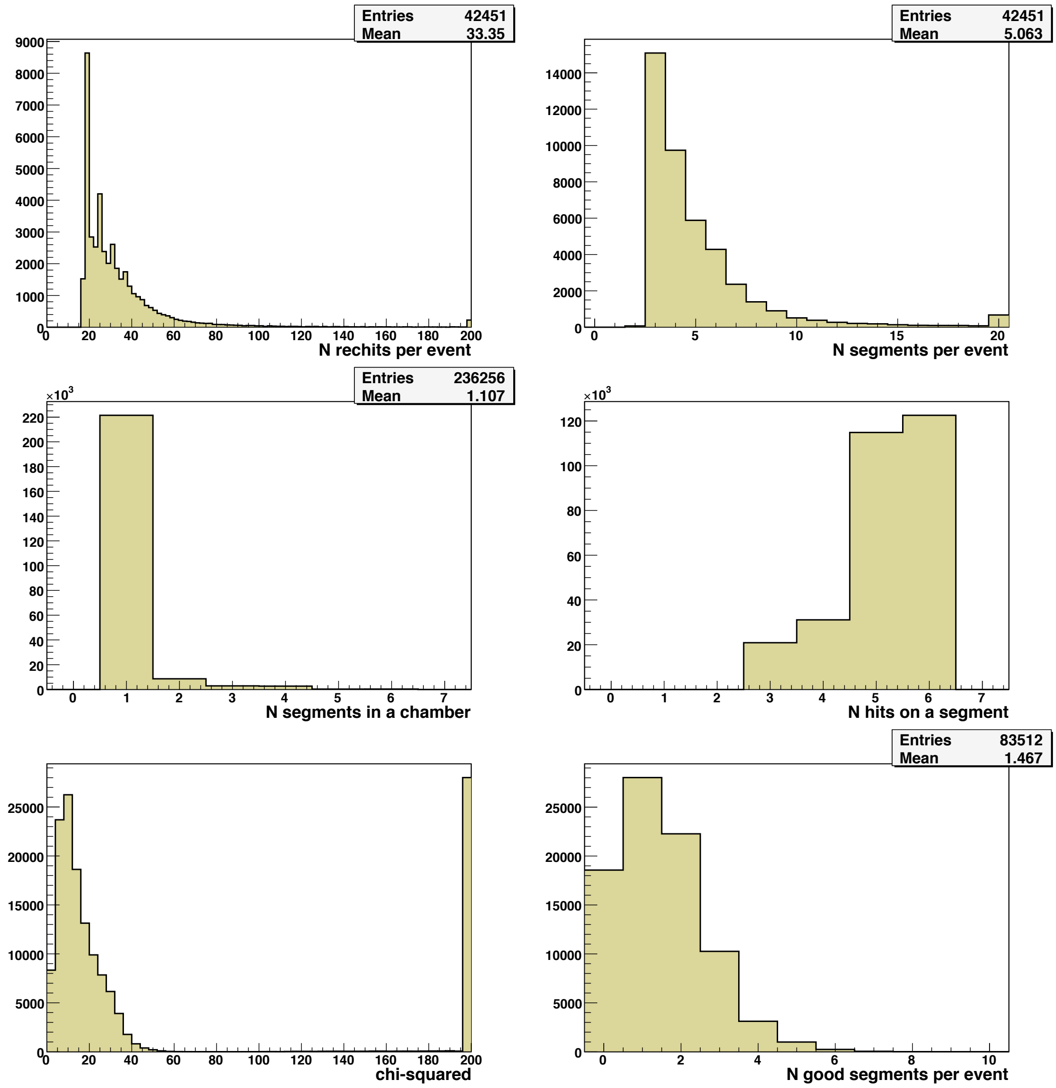

Figure 14: distributions of basic quantities used in event selection

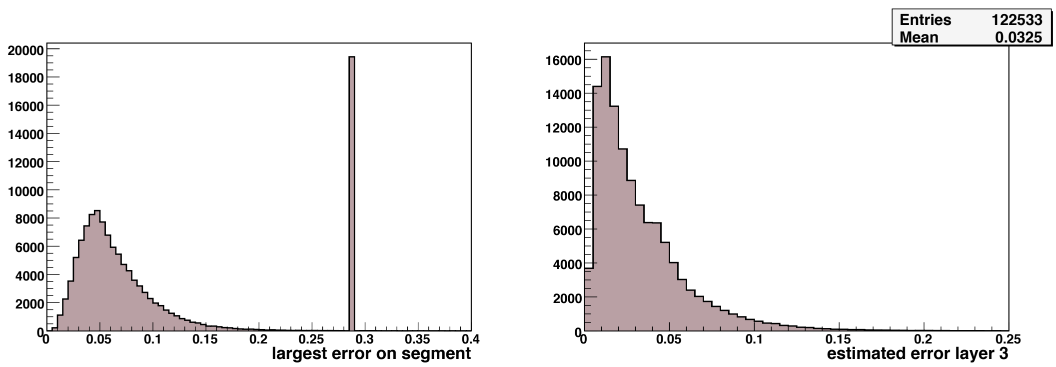

Figure 15: *Left:* largest estimated error for all rechits on a segment. A segment is rejected if this largest error is larger than 0.2. *Right:* the estimated error for selected rechits in layer 3.

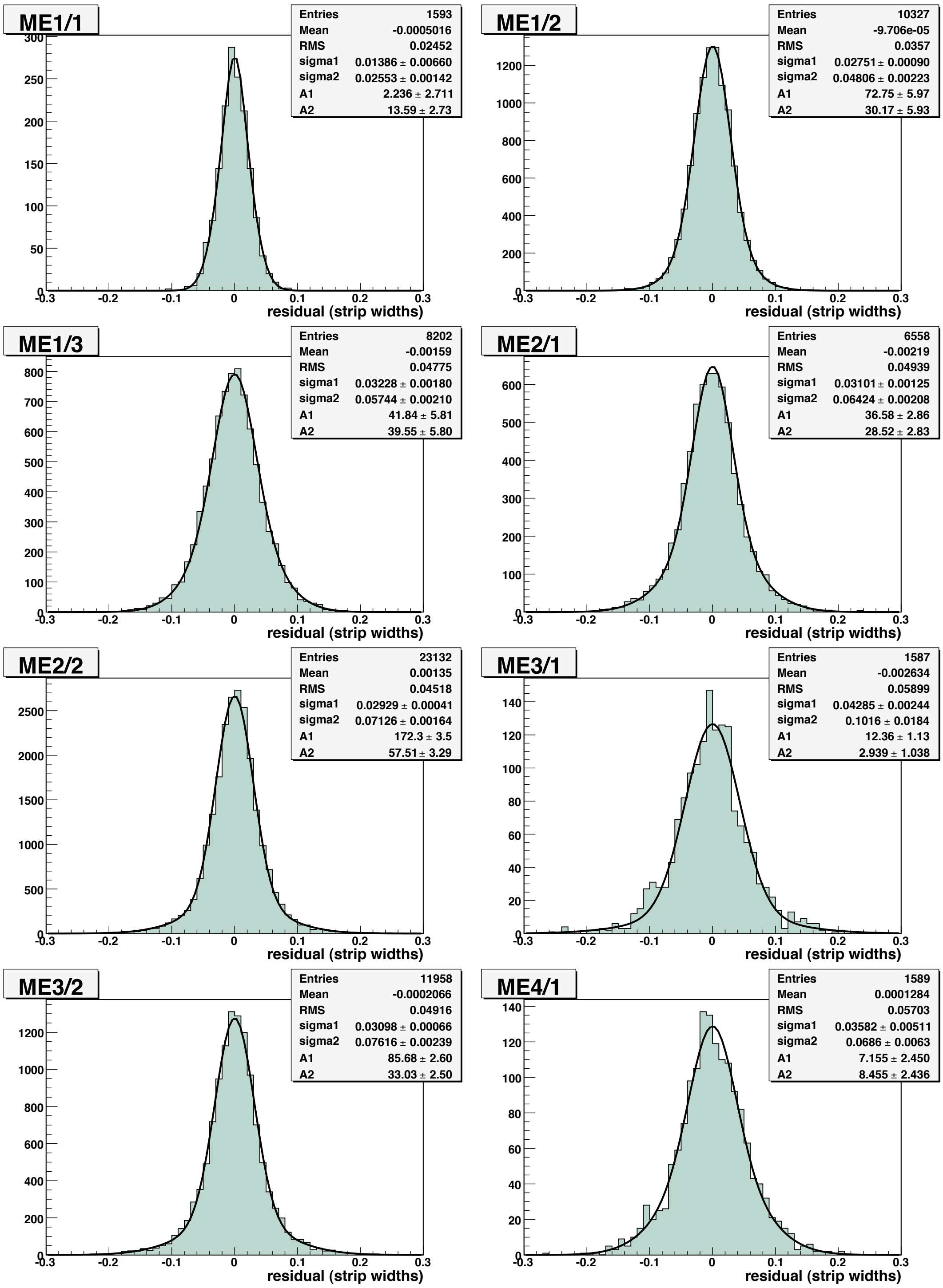

Figure 16: residuals distributions fit to the double-Gaussian function given in Eq. 7.

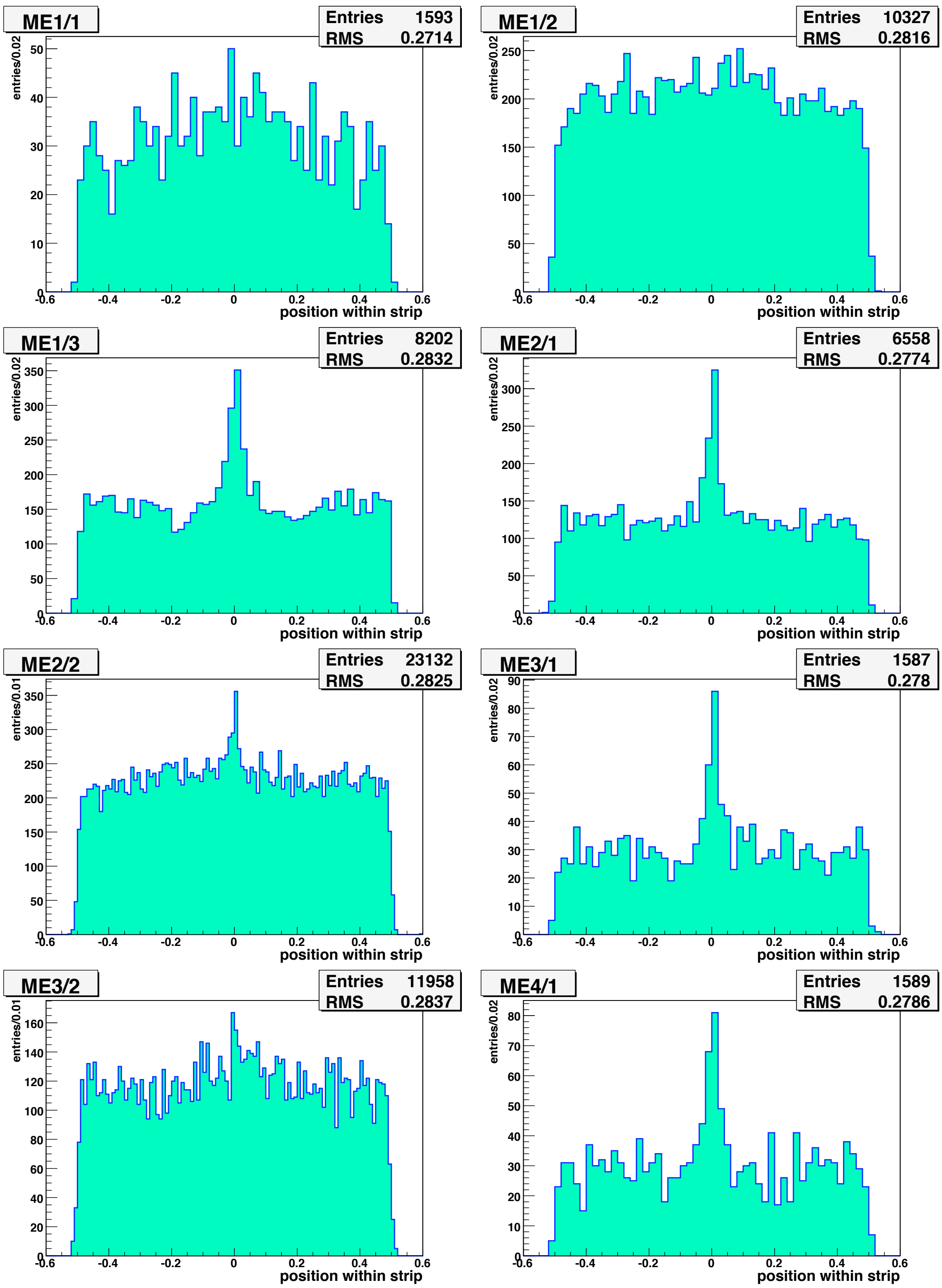

Figure 17: distributions of strip coordinates, s, for all chamber types

chamber	$\langle Q_{3\times3}\rangle$	r.m.s. pedestal width
ME±1/1	926	2.26
ME±1/2	796	2.00
ME±1/3	822	2.27
ME±2/1	745	2.08
ME±2/2	782	2.80
ME±3/1	723	2.05
ME±3/2	784	2.81
ME±4/1	724	1.93

Table 5: mean $Q_{3\times3}$ and the r.m.s. pedestal width, ascertained from `CSCValidation` plots for CRAFT run 68100. Numbers are in ADC counts.

[5] S. Durkin, T. Ferguson and N. Terentiev, *Validation of the Simulation of the CMS Endcap Muon Cathode Strip Front-end Electronics*, CMS-AN/2005-066

OTHER TESTBEAM STUDIES. (Above cite is not the right one...)

[6] V. Barashko et al., *Unpacking and Reformatting the CSC Raw Data*, CMS-IN/2009-009

I. Bloch et al., *CSC Segment Reconstruction: ST Algorithm – A Spanning Tree Approach*, CMS-IN, submitted

[7] S. Stoynev et al., *Rechit Reconstruction in the CSC's*, CMS-IN, in preparation

[8] S. Stoynev and M. Schmitt, *Efficiency Measurements in the CSC Muon Endcap System*, CMS-NOTE, in preparation

[9] CMS Collaboration, *Studies of CMS Muon Reconstruction Performance with Cosmic Rays*, in preparation

G. Abbiendi et al., *Muon Reconstruction in the CMS Detector*, CMS-AN/2008-097

[10] E. Gatti et al., *Optimum Geometry for Strip Cathodes or Grids in MWPC for Avalanche Localization Along the Anode Wires*, Nucl. Instrum. Meth. **163** (1979) 83

[11] E. Mathieson and J. Gordon, *Cathode Charge Distributions in Multiwire Chambers: I. Measurement and Theory*, Nucl. Instrum. Meth. **227** (1984) 267; *op. cit., II. Approximate and Empirical Formulae*, Nucl. Instrum. Meth. **227** (1984) 277

[12] V. Perelygin et al., *ME1/1 CSC Spatial Resolution*, CMS NOTE, submitted.

[13] A. Kubik et al., *The CSCValidation Program*, CMS-IN, in preparation